Cellulose (2024) 31:2815–2832
https://doi.org/10.1007/s10570-024-05793-0

ORIGINAL RESEARCH

Making fibers from cellulose derivatives by pressurized gyration and electrospinning

Nanang Qosim · Hamta Majd · Jubair Ahmed · Gareth Williams · Mohan Edirisinghe

Received: 9 January 2024 / Accepted: 3 February 2024 / Published online: 4 March 2024

Abstract Cellulose derivatives are obtained from renewable sources, making them an environmentally friendly option in many industrial applications. Manufacturing fine cellulose fibers is confronted with multifaceted challenges due to cellulose's intricate nature, such as its highly organized structure and hydrogen bonding chain. In this study, for the first time, fibers in the nanometer to micrometer scale diameter from cellulose derivatives were successfully produced without the assistance of polymer precursors using the pressurized gyration (PG) technique. The cellulose derivatives investigated in this work were ethyl cellulose (EC) and cellulose acetate (CA), representing the ether and ester cellulose derivatives, respectively. Electrospinning (ES) technique was also used to compare the fibers produced by this technique with those produced by PG. Both PG and nozzle-PG succeeded in producing EC-based fibers with diameters ranging from 488 to 825 nm, with a higher production rate than ES. In contrast, ES succeeded in producing bead-free fibers from EC and CA with a wide range of solvent systems and concentrations. Scanning electron microscopy was used to analyze the fiber morphology, diameter distribution, and alignment. Additionally, Fourier transform infrared spectroscopy, x-ray diffraction, and differential scanning calorimetry were used to compare the physicochemical nature of the fibers produced by PG and ES. These tests revealed that the fibers produced from the two spinning methods had identical physicochemical structures and properties. With further research and development efforts, PG has the potential to be a promising technique for producing cellulose derivative-based fibers with a high production rate, which could be employed for applications in drug delivery, tissue engineering, and wound dressing.

Keywords Ethyl cellulose · Cellulose acetate · Pressurized gyration · Electrospinning · Fibers

N. Qosim · H. Majd · J. Ahmed · M. Edirisinghe (✉)
Department of Mechanical Engineering, University College London, London WC1E 7JE, UK
e-mail: m.edirisinghe@ucl.ac.uk

N. Qosim
Department of Mechanical Engineering, Politeknik Negeri Malang, Jl. Soekarno Hatta No.9, Malang, Jawa Timur 65141, Indonesia

N. Qosim · G. Williams
UCL School of Pharmacy, University College London, 29-39 Brunswick Square, London WC1N 1AX, UK

Introduction

The term "green" polymer is associated with those derived from natural materials. It represents an environmentally friendly alternative to synthetically produced materials as they reduce the amount of non-biodegradable waste (Oprea and Voicu 2020). Cellulose and its derivatives are considered "green" polymers due to their renewable nature,

biodegradability, non-toxicity, and potential for environmentally friendly processing. These "green" polymers can be obtained from a wide range of sources, such as the cell walls of plants, certain types of algae and bacteria, and tunicates, which are the only creatures containing cellulose (Chavooshi et al. 2023; Seddiqi et al. 2021). Owing to their outstanding properties, cellulose derivatives are widely studied for various applications in their numerous forms (Oprea and Voicu 2020; Shaghaleh et al. 2018).

In this work, ethyl cellulose (EC) and cellulose acetate (CA) are chosen because they are a few of the widely used cellulose derivatives for producing fiber. EC is a cellulose ether that is generally considered non-toxic and biocompatible and has several advantages when utilized as fibers. Due to its low water solubility and its ability to encapsulate and protect active substances, EC fibers are commonly utilized in drug delivery systems and other encapsulation applications (Gençtürk et al. 2020; Godakanda et al. 2019; Wang et al. 2023). CA is an acetate ester of cellulose created by acetylation (Angel et al. 2020), where some of the hydroxyl groups in the cellulose chain are replaced with acetate groups. This chemical modification makes CA more soluble in certain organic solvents and provides it with distinct properties. CA is known to be able to produce micro and nanofibers through various fabrication methods. CA fibers have been reported to have advantages in tissue engineering scaffolds and drug delivery systems (Chen et al. 2020; Sofi et al. 2021).

Although various methods of fabricating cellulose-derived fibers have been developed recently, this topic remains important and challenging. Cellulose is a polysaccharide that is not readily dissolved in common organic solvents or easily melted (Jayawardena et al. 2017), making it more challenging to process using standard fiber manufacturing techniques such as electrospinning. Additionally, a notable limitation of electrospinning is its relatively low production rate, which hinders its scalability for industrial use (Wang et al. 2016). Rao et al. succeeded in fabricating EC fiber with diameters ranging from 1.69 to 3.68 µm using the facile method, microfluidic spinning. However, the EC fiber fabrication required polyvinylpyrrolidone (PVP) to make its spinnability feasible (Rao et al. 2022). Another method, solution blow spinning, was also reported successful in spinning CA fiber by Dadol et al. (2020). However, using this method, an easily spun polymer precursor, polyacrylonitrile (PAN), was also needed to spin CA.

Pressurized gyration (PG), a strategy for producing polymer fibers, combines centrifugal spinning and solution blowing (Mahalingam and Edirisinghe 2013). It was developed to overcome significant electrospinning (ES) limitations, such as typically low production rates, challenges in process optimization, and the requirement for large electrical voltages. PG (apparatus depicted in Fig. 1) affects the polymer solution's instability due to the Rayleigh–Taylor interaction. The polymer solution is displaced because of the increased centrifugal force as the vessel spins. The applied gas pressure pushes

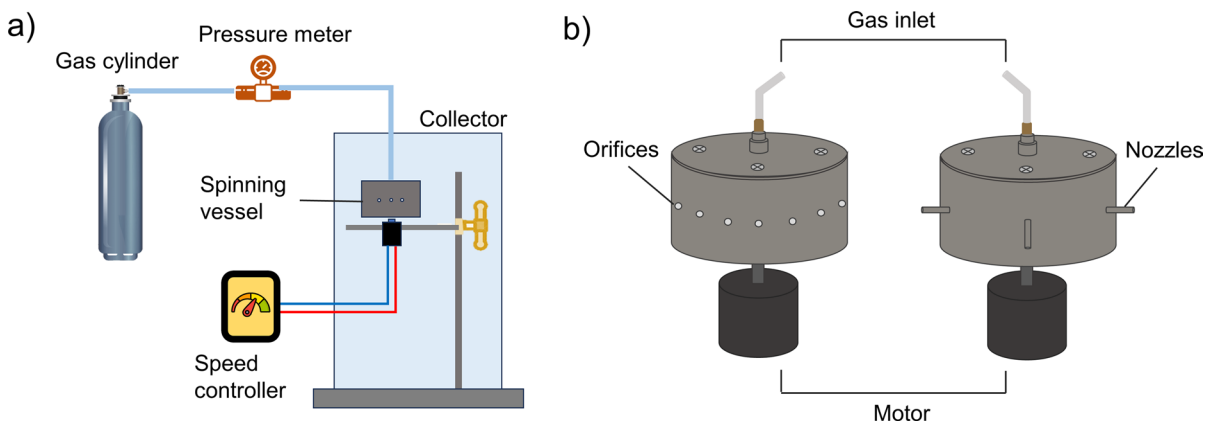

Fig. 1 **a** Experimental setup of pressurized gyration; and **b** details of the spinning vessel used for PG (with orifices) and N-PG (with nozzles)

the liquid out of the vessel, producing a pressure differential (Heseltine et al. 2018; Mahalingam et al. 2015). A liquid–air surface tension gradient produces a concentrated polymer jet. This gradient additionally induces a Marangoni stress perpendicular to the liquid–gas interface that drives the movement of polymer droplets. Once the solvent evaporates, the extruded polymer in the jet becomes a fiber strand. As the internal pressure of the gas applied in PG increases, so does the pressure difference between the interior and exterior liquid–air interfaces. This increases the force applied as the polymer jet is extruded through the orifices, resulting in increased jet thinning and, consequently, finer deposited fibers (Kelly et al. 2022). Nozzle-pressurized gyration (N-PG) is a new PG process developed by Dai et al. (2022), by replacing the 24 orifices in the PG vessel with four directional nozzles. In the N-PG, the discharged polymer solution is directed by the nozzles (Fig. 1b, right). Accordingly, it enhances the orientation and uniformity of the fibers produced. Research revealed that the N-PG had an advantage in producing homogeneous fibers with reduced diameters and improved alignment over the PG while maintaining the same production yield (Dai et al. 2022).

To the best of current knowledge, there are no reported studies on the facile fabrication of cellulose derivatives without the assistance of additives using the PG method. Using PG, Brako et al. succeeded in producing bioadhesive progesterone-loaded nanofibers with polyethylene oxide (PEO) and carboxymethyl cellulose (CMC) as polymers. However, in their work, only 1.25 wt% of CMC was incorporated into 13.75 wt% of PEO (Brako et al. 2018). In another study investigated by Altun et al., bacterial cellulose (BC) fiber was also successfully fabricated using the PG method with the assistance of poly(methylmethacrylate) (PMMA) polymer at various ratios. However, only a small concentration of BC, 5:50 BC:PMMA composition, offered the best compromise in terms of fiber morphology and quality (Altun et al. 2018). Therefore, this study aims to fill that gap by fabricating cellulose derivative fibers without the help of additives and surfactants using the PG method. This study is anticipated to provide an alternative for manufacturing cellulose derivative fibers with a higher production rate compared to conventional methods.

Experimental details

Materials

Ethyl Cellulose (EC, 48% ethoxy, Mw 448.483 g mol^{-1}, CAS: 9004-57-3) and Cellulose Acetate (CA, 39.8% acetyl, Mw 30,000 g mol^{-1}, CAS: 9004-35-7) were purchased from Sigma-Aldrich (Gillingham, UK). The following solvents were also purchased: ethanol absolute (CAS: 64-17-5, Mw 46.07 g mol^{-1}) from VWR Chemicals (Strasbourg, France), chloroform ≥ 99.5% (CAS: 67–66-3), N,N-dimethylacetamide ≥ 99% (DMAc, CAS: 127–19-5, Mw 87.12 g mol^{-1}), tetrahydrofuran ≥ 99.9% (THF, CAS: 109–99-9, Mw 72.11 g mol^{-1}) and acetone ≥ 99.5% (CAS: 67-64-1, Mw 58.08 g mol^{-1}) from Sigma-Aldrich (Gillingham, United Kingdom). All analytical-grade materials were utilized in their original form.

Solution preparation and characterization

For each polymer, three different concentrations were used in this work: 5, 10, and 15% weight over volume (w/v). The concentration range was selected based on its ability to generate EC and CA solutions with a viscosity suitable for both PG and ES. Each concentration was dissolved in various types of solvent or binary solvent system, as shown in Table 1. All polymer solutions were stirred using a magnetic stirrer (MS7-H550-Pro, DLAB, USA) with a speed of 240 RPM at 16–18 °C ambient temperature for 24 h until a homogenous solution formed. Prior to the fabrication process using the PG, N-PG, and ES methods, all tested solutions were first characterized for their physical properties, including viscosity and surface tension, two important properties of fluids that significantly influence the morphology of the resulting fiber. Using a programmable rheometer (DV-III Ultra, Brookfield Engineering Laboratories Inc, Massachusetts, USA), the viscosity of each solution was determined. The surface tension of the solutions was characterized via a tensiometer (Tensiometer K9, Kruss GmbH, Germany). For this purpose, the Wilhelmy plate method was applied. Each sample was measured three times for each viscosity and surface tension test, and the variation was calculated and given.

Table 1 Polymer solutions and their properties used in this study

Polymer	Concentration (w/v)	Solvent	Abbreviation	Viscosity (mPa s)	Surface tension (mN m^{-1})
EC	5	Ethanol	5EC-EtOH	368 ± 3	22.10 ± 0.7
		Chloroform	5EC-Chl	242 ± 4	27.24 ± 0.4
		DMAc:THF at 1:1 (v/v)	5EC-DMAc:THF	186 ± 3	30.04 ± 0.4
	10	Ethanol	10EC-EtOH	1267 ± 11	23.32 ± 0.6
		Chloroform	10EC-Chl	1008 ± 9	29.86 ± 0.8
		DMAc:THF at 1:1 (v/v)	10EC-DMAc:THF	564 ± 6	31.72 ± 0.3
	15	Ethanol	15EC-EtOH	2215 ± 27	24.09 ± 0.4
		Chloroform	15EC-Chl	2175 ± 31	31.95 ± 0.5
		DMAc:THF at 1:1 (v/v)	15EC-DMAc:THF	1236 ± 18	32.44 ± 0.7
CA	5	Acetone: DMAc at 5:1 (v/v)	5CA-Ace:DMAc	32 ± 1	24.87 ± 0.6
		DMAc:THF at 1:1 (v/v)	5CA-DMAc:THF	55 ± 2	29.22 ± 0.8
		Acetone: Distilled water at 5:1 (v/v)	5CA-Ace:DW	32 ± 2	27.92 ± 0.8
	10	Acetone: DMAc at 5:1 (v/v)	10CA-Ace:DMAc	66 ± 2	26.35 ± 0.5
		DMAc:THF at 1:1 (v/v)	10CA-DMAc:THF	142 ± 4	29.99 ± 0.6
		Acetone: Distilled water at 5:1 (v/v)	10CA-Ace:DW	70 ± 3	29.58 ± 0.4
	15	Acetone: DMAc (5:1)	15CA-Ace:DMAc	223 ± 3	27.21 ± 0.4
		DMAc:THF at 1:1 (v/v)	15CA-DMAc:THF	676 ± 3	30.85 ± 0.7
		Acetone: Distilled water at 5:1 (v/v)	15CA-Ace:DW	646 ± 4	31.44 ± 0.6

Experimental setup for pressurized gyration and nozzle-pressurized gyration

In the PG and N-PG experiments, 3 mL of the solutions were loaded into the spinning vessel before PG was undertaken at the specified operating pressure and collecting distance. A schematic diagram of the PG and N-PG methods is illustrated in Fig. 1. In the first phase, the PG and N-PG operating conditions included the pressurized nitrogen gas infusion at 0.3 MPa and continuous vessel rotation at 6000 RPM (the speed of the motor with the vessel applied). To study the effect of parameter optimizations of the PG, firstly, three different gas pressures of 0.1, 0.2, and 0.3 MPa were applied while maintaining the vessel rotation at 6000 RPM. Secondly, with constant gas pressure at 0.3 MPa, three different vessel rotations, 1800, 5000, and 8500 RPM, were applied. The spinning process was conducted at 16.8–18.2 °C and 47–48.5% relative humidity, with the collection distance set at 80 mm.

Experimental setup for electrospinning

In the electrospinning experiment, 5 mL of the solution was loaded into a 10 mL syringe (Terumo Corporation, Tokyo, Japan) and connected to a stainless-steel needle with capillary tubing, as illustrated in Fig. 2. The polymer flow rate was regulated using

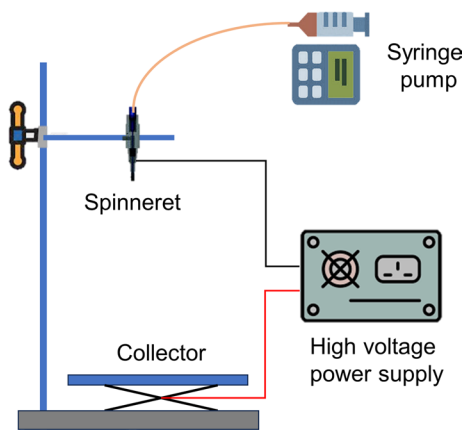

Fig. 2 Experimental setup of electrospinning

a syringe pump (PHD 4400 Programmable, Harvard Apparatus, Edenbridge, UK). The needle was connected to a high-precision DC power supply (Glassman High Voltage Inc., New Jersey, USA) with an output range of 0–30 kV. A grounded electrode was connected to the metal collector. The distance between the spinneret and the collector was 150 mm. The flow rate and the voltage applied are 0.1 mL min^{-1} and 20 kV, respectively. All experiments were conducted at 21.3–22.2 °C and 44.1–46.2% relative humidity.

Fiber characterization

Morphology

The morphology of the fibers was investigated using an SEM (GeminiSEM 360, Carl Zeiss Microscopy GmbH, Oberkochen, Germany) with a 1–10 kV acceleration voltage. Image analysis software, ImageJ, was used to calculate the average fiber diameter and size distribution from the micrographs produced by SEM imaging. In this investigation, 100 fiber strands were randomly selected for each fiber sample. The average diameter of the fibers was estimated and displayed using Origin Pro graphing software. Using the fiber diameter information, a comparison was made between various solvents, concentrations, and setup parameters.

The scanning electron micrographs were also used to compare the alignment of fibers by determining the coherence coefficient. An additional plugin for ImageJ, OrientationJ, was utilized to calculate the directional coherence coefficient of the fibers. The structure tensor was used to calculate the coherency. A histogram of the orientation was then generated, considering only the pixels with a coherency greater than a specified minimum coherency. The histogram was weighted, with the weight being the coherency value itself. The minimum coherency was expressed as a percentage since the coherency factor ranged from 0 to 1 (Rezakhaniha et al. 2012).

Physicochemical properties

The characterization of physicochemical properties was carried out using Fourier transform infrared spectroscopy (FTIR), X-ray diffraction (XRD), and differential scanning calorimetry (DSC). The characterization aimed to compare the fiber properties produced using the PG and ES methods. Therefore, observations were only made on formulations that could produce fiber using both PG and ES methods. In the FTIR test, 2 mg of each sample was placed on the ATR crystal of the spectrometer (Nicolet iS50, Thermo Scientific, Massachusetts, USA) and analyzed over 10 cycles in the range of 4,000–500 cm^{-1} at a resolution of 4 cm^{-1}.

The XRD patterns of pressure-spun and electrospun fibers were analyzed using a MiniFlex 600 instrument (Rigaku, Tokyo, Japan) diffractometer system equipped with a Cu-Kα radiation source. Fiber samples were placed into specimen holders and analyzed in the 2θ range between 3 and 40°. The scan rate and step size were 1.0°/min and 0.05°, respectively.

DSC analysis was conducted using a STARe System DSC 3 (Mettler Toledo, Ohio, USA). A 5 mg sample of the fiber sample was sealed in an aluminum pan. On the other hand, a blank pan was prepared as a reference. The sample and the reference were then placed into a sample holder, aluminum standard 40 µL, and then heated from 0 to 300 °C at 10 °C min^{-1} under a nitrogen flow.

Results and discussion

Pressurized gyration and nozzle-pressurized gyration

Ethyl cellulose

Table 1 shows that EC was successfully dissolved in various solvents: ethanol, chloroform, and a binary solvent system of DMAc and THF. The solutions produced from three different solvents had different viscosity and surface tension values, even though the EC concentrations were kept the same. The concentration increases because there are a higher number the polymeric. EC molecules tend to interact and entangle with each other, as well as with solvent molecules. This intermolecular interaction increased flow resistance, leading to higher viscosity (Wu et al. 2017). Besides that, at higher concentrations of EC, the polymer chains can be increasingly entangled, forming a network-like structure within the solution (Mehta and Pawar 2018). The entangled polymer chains restrict the movement of solvent molecules.

Despite the solutions having high viscosity, with ethanol and chloroform as solvents, it was not possible to produce fibers, although these solvents are among the most widely used to generate fibers from numerous polymers. The spinnability of a solution to form fibers in PG is greatly influenced by its intrinsic characteristics, including molecular structure and weight, crystalline nature, concentration, viscosity, surface tension, and solvent evaporation rate, which in turn affect the morphology and structure of the resulting fibers (Dai et al. 2023). Careful consideration is required in choosing solvents for producing fibers within polymer–solvent systems (Heseltine et al. 2018).

For the first time, EC fibers were successfully produced using the PG and N-PG methods, as shown in Fig. 3. In this work, the binary solvent system of DMAc and THF provided sufficient solution parameters to produce fibers from EC with a concentration of 10% or 15%. The concentration of polymer in a solution significantly influences fiber production in PG. There is a crucial threshold concentration that must

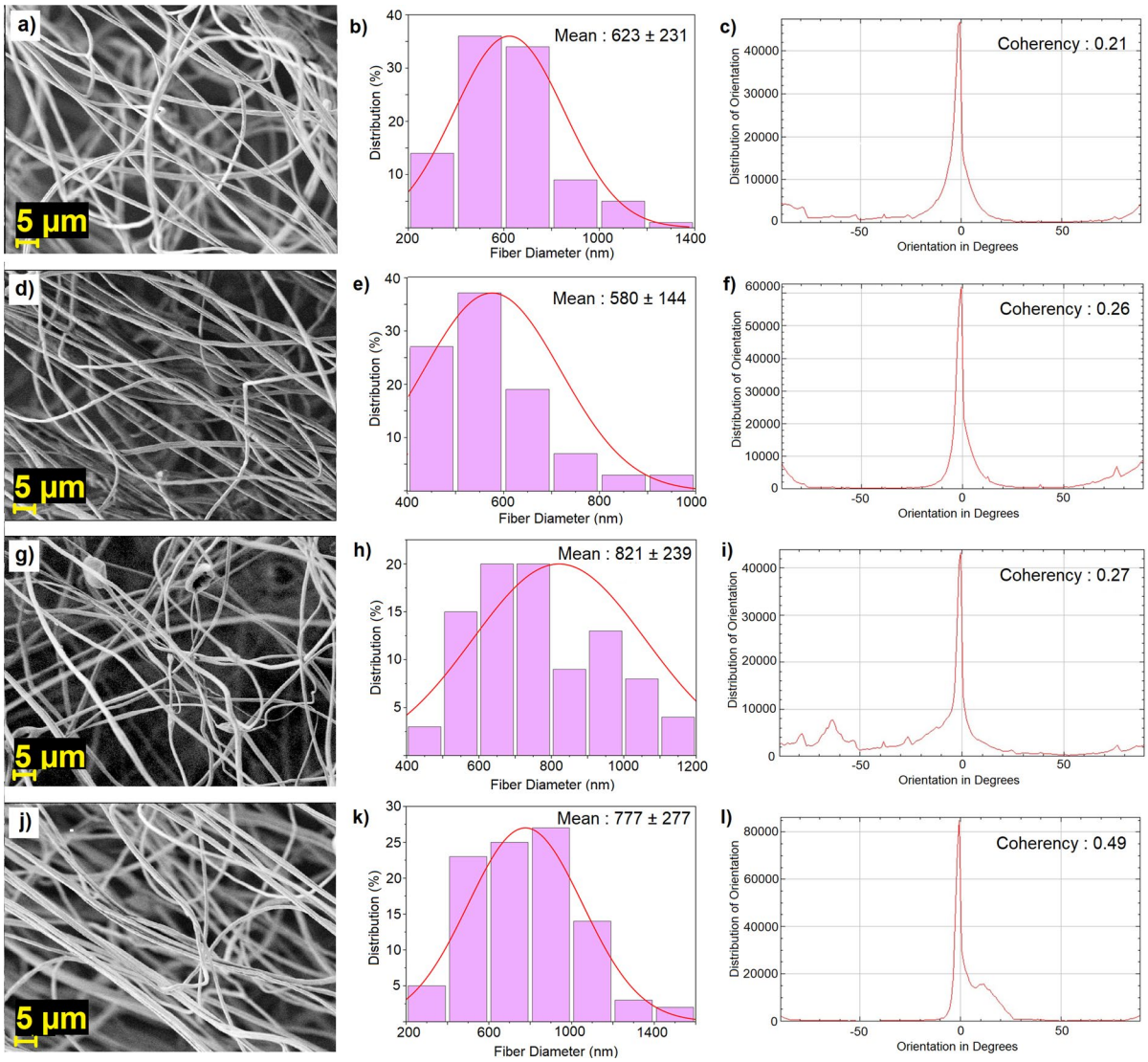

Fig. 3 Scanning electron micrographs, size distribution histograms, and orientation distribution graphs of EC fibers fabricated by **a–c** PG 10EC-DMAc:THF; **d–f** N-PG 10EC-DMAc:THF; **g–i** PG 15EC-DMAc:THF; and **j–l**) N-PG 15EC-DMAc:THF

be reached for fiber production to occur. Once this minimum concentration is surpassed, the polymer molecules become sufficiently entangled, preventing the jet from breaking apart during the spinning process.

As for the 5% concentration, the resulting viscosity was insufficient to produce fibers with PG. Polymeric viscosity is a critical factor in PG. Higher viscosity solutions tend to form fibers more readily as they offer opposing resistance to flow, allowing for better elongation and fiber formation, as well as sufficient polymer chain entanglement. In contrast, less viscous solutions have lower resistance to flow, making it challenging to form fibers under the centrifugal and shearing forces of PG. If the viscosity of the solution is insufficient, it may not provide sufficient resistance to stretching and elongation. As a result, the solution may be more prone to fragmenting into droplets or beads rather than forming continuous fibers.

Figure 3a shows that the PG method with a parameter setup of 6000 RPM and 0.3 MPa pressure produced fibers with a diameter of around 623 nm from EC with a concentration of 10%. Apart from having a bead-on-string morphology, the generated fibers had good uniformity. As a comparison, in this study, the same solution was also successfully spun by the N-PG method with the same parameters. With the N-PG method, the resulting fibers had a slightly smaller diameter of 580 nm. By modifying the orifices to nozzles, the fibers generated improved alignment, as shown in Fig. 3b. This is confirmed by the coherence coefficient of 0.26, greater than the fiber coherence coefficient produced by the original PG method, which is 0.21. Theoretically, the greater the coherence coefficient (the closer it is to 1), the better the level of alignment (Young et al. 2019).

Furthermore, Fig. 4 summarizes the production rate of EC in the PG and N-PG. For EC with a concentration of 10%, the associated fiber yield was 12.3 mg per 1 mL solution or 12.3% of solute (there are 100 mg solute in 1 mL solution). Empirically, 3 mL of solutions could be spun for 10 s in PG, therefore, the production rate of this process was theoretically 221.4 mg min^{-1} for this polymer system. Unfortunately, apart from these advantages, the N-PG yielded less product than the PG, at only 10.4% of solute.

Similar results were obtained from the EC solution with a concentration of 15%, as shown in Fig. 3c and d. At this concentration, PG produced fibers with a diameter of 821 nm and a coherence coefficient of 0.27. In comparison, the N-PG managed a smaller diameter (777 nm), with almost double the coherence coefficient (0.49). Overall, N-PG generated EC fibers with a higher uniformity and alignment for all concentration. This result can be elucidated by examining the stability of spinning jets. Despite following a similar trajectory post-extrusion from the spinning vessel in both PG and N-PG, which includes processes like jet necking and whipping, there are differences in the direction of jet ejection and the flow characteristics of the polymer solution. In PG, the gas outflow from the orifices resembles a jet. Additionally, turbulence arises due to the fluctuating pressure when the polymer fluid is expelled through the orifices. Consequently, polymer jets may form at varying angles to the central axis of the orifice, resulting in differing initial jet diameters, which accounts for the lower fiber alignment and uniformity. On the contrary, directing the liquid through nozzles assists in stabilizing the flow state of the polymer and forming steady spinning jets. Ultimately, polymer jets exiting the nozzle exhibit a more stable flow state and tend to follow the nozzle axis due to inertia, consequently enhancing fiber alignment and uniformity (Dai et al. 2022).

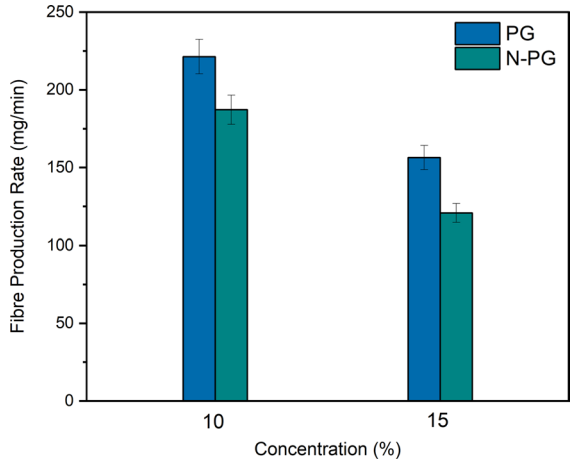

Fig. 4 The production rate of EC-(DMAc:THF) fiber produced via PG and N-PG

Surprisingly, as shown in Fig. 4, increasing the solution concentration decreased the fiber yield drastically for both PG and N-PG. To some extent, a higher polymer concentration should make spinning

easier and increase the yield of fibers (Kelly et al. 2022). However, increasing the EC concentration to 15% raised the viscosity of the solution, which could inhibit solvent evaporation. This inhibition will result in a solidification process that will occur sooner during spinning, which can result in a failure of fiber formation (Mahalingam and Edirisinghe 2013). Moreover, increasing the EC concentration tends to produce fibers with a thicker diameter. This is because a higher concentration of the polymer leads to an increase in the polymer chains present in the solution, allowing for a greater number of polymers to be spun. Additionally, a higher polymer concentration will impose higher resistance against the destabilizing centrifugal force, leading to dynamic fluid blowing, thereby encouraging the production of fibers with a thicker diameter (Mahalingam et al. 2020).

Cellulose acetate

The CA solution could not produce any fibers with the PG or N-PG methods using any of the solvents and concentrations explored. At concentrations of 5% and 10%, the viscosity of the solutions resulted from all solvent systems was very low, only ranging between 32 and 142 mPa s. This lower viscosity compared to EC at the same concentration is caused by the CA molecular weight being much lower than the EC molecular weight. As explained previously, lower solution viscosities may not provide sufficient resistance to stretching and elongation for fiber formation. Even with sufficient viscosity to undergo PG and N-PG, 15CA-DMAc:THF or 15CA-Ace:DMAc solution placed in the vessel was only ejected from the orifices and nozzles as droplets as a result of insufficient evaporation of solvent.

However, this failure is very complicated, because the process of fiber formation in PG is determined by several factors at the same time. The interplay between centrifugal force, pressure difference at the orifice, and surface tension of the CA solution drives fiber formation in this process (Mahalingam and Edirisinghe 2013). Given the intricate nature of the CA structure and properties there are several examples of approaches which have successfully produced fibers from several unspinnable or difficult to spin polymers which may be applicable. Recently, Dai et al. made modifications to a standard N-PG device in order to address the issue of spinning jets not forming a structured entity before being collected when spinning cellulose solutions. They introduced a coagulation bath into the N-PG setup, which was used in the wet spinning process (Dai et al. 2024). Their work succeeded in producing cellulose fiber which could not be done using conventional PG methods. Another method that might be applied is to increase the solvent evaporation rate. This can be done by involving the additional heating as done by Kelly et al. to increase the spinnability of cyclodextrin with PG (Kelly et al. 2022). The fabrication of CA fibers with PG still needs further investigation to find the right combination of solvent solubility and spinnability or adjustments to spinning parameters.

Effect of process control parameters on pressure-spun fibers

As mentioned previously, EC was the only cellulose derivative that could successfully produce fibers with PG in this work, with the greatest yield obtained at a concentration of 10% with the THF:DMAc solvent system. Therefore, an investigation was carried out to observe the effect of the setup parameters, including gyration speed (RPM) and gas pressure (MPa), on the pressure-spun fibers produced. The morphology and diameter of the fibers produced with the optimization of gas pressure are depicted in Fig. 5. At a constant gyration speed of 6000 RPM and an applied gas pressure of 0.1 MPa, the PG produced fibers with a diameter of 825 nm, as shown in Fig. 5a. It is clear that this diameter decreased with increasing gas pressure, where the smallest diameter of 528 nm was obtained (Fig. 5b and c) by applying a maximum pressure of 0.3 MPa. This decrease can be explained by the fact that applying a higher gas pressure increased solvent evaporation during spinning. The higher the evaporation rate, the smaller the diameter of the fibers produced. Unfortunately, although the smaller fibers could be produced, the increased pressure resulted in instability, aggravating fiber uniformity.

In addition to pressure, a critical minimum gyration speed must be met to produce fibers from the polymer solutions. Therefore, three gyration speeds, 1800, 5000, and 8500 RPM, were applied with a constant gas pressure of 0.3 MPa. The micrographs of these fibers and their diameter distribution are depicted in Fig. 6. At a gyration speed of 1800 RPM, the EC solution with a concentration of

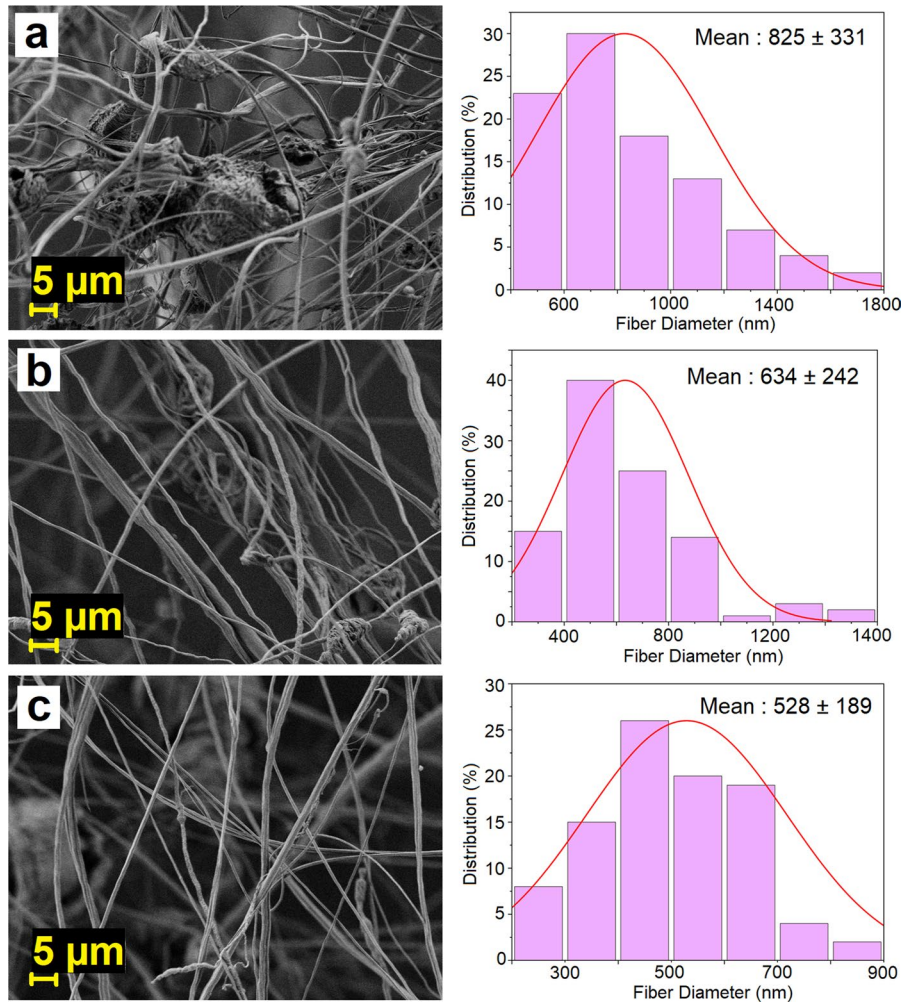

Fig. 5 Scanning electron micrographs and size distribution histograms of optimized pressure-spun fibers with different gas pressure: **a** 0.1 MPa, **b** 0.2 MPa, and **c** 0.3 MPa

10% produced fibers with an average diameter of 622 nm. This diameter decreased to 559 nm when the gyration speed was increased to 5000 RPM. At a gyration speed equal to 8500 RPM, the resulting fiber diameter decreased to 488 nm.

Another observation that stands out is the poor fiber uniformity at a gyration speed of 8500 RPM, as shown in Fig. 6c, caused by the instability at higher gyration speeds. Theoretically, increasing the gyration speed will increase the centrifugal force on the PG pot. A reduction in fiber diameter will occur with a rise in gyration speed because, like an increase in gas pressure, an increase in gyration speed also tends to increase the solution's evaporation rate (Heseltine et al. 2018).

Electrospinning

Ethyl cellulose

ES was also studied to compare the spinnability of solutions that had been successfully dissolved. Several EC solutions could be electrospun successfully, and the morphology of the resulting products is displayed in Fig. 7. For the EC solution with ethanol as the solvent, the concentrations of the solution that could be electrospun were 5% (Fig. 7a) and 10% (Fig. 7b). However, for solution concentration of 15%, the very high viscosity made ES unsuccessful. The fiber morphology of the 5% solution showed a number of "beads on string" compared to the fibers

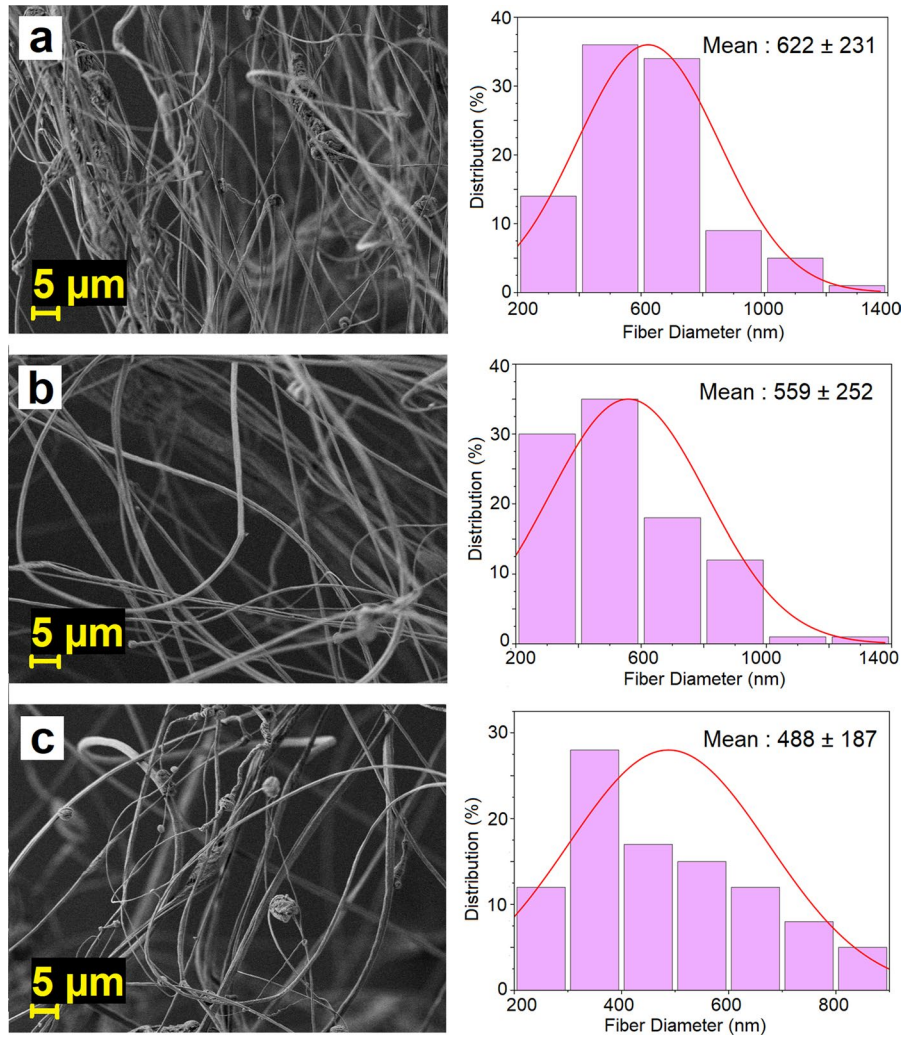

Fig. 6 Scanning electron micrographs and size distribution histograms of optimized pressure-spun fibers with different gyration speeds: **a** 1800 RPM, **b** 5000 RPM, and **c** 8500 RPM

produced from the 10% EC solution. This was due to the former solution's low concentration, which failed to achieve sufficient chain entanglement, the physical interlocking of polymer chains (Husain et al. 2016). Ethanol has relatively high volatility, and a fast evaporation rate can lead to rapid solvent removal during the ES process. When the solvent evaporates too rapidly, the polymer chains may not be allowed sufficient time to align and solidify into continuous fibers. Instead, small droplets of the polymer solution may solidify into beads along the fiber's length.

With ethanol as a solvent, ES could produce very thin fibers within the nanometer scale, namely 68 nm for a solution with a 5% EC concentration and 228 nm for 10%. These two values were much thinner than the fibers produced with the binary solvent system of DMAc:THF. The production of very thin fibers was also because of the rapid evaporation of ethanol. During ES, as the EC solution was ejected from the spinneret, the rapid evaporation of ethanol caused it to dissipate from the polymer jet quickly. This rapid evaporation facilitated the solidification of the EC polymer, forming thinner EC fibers. Moreover, based on the surface tension data in Table 1, ethanol provided a lower surface tension, which could help reduce the formation of larger droplets during ES (Ajith et al. 2023). Smaller droplets were more likely to elongate into thinner EC fibers as they were subjected to the electric field and the stretching forces of ES. According to previous studies, the small fiber diameter significantly enhances the available surface area-to-volume ratio. This is beneficial for tissue

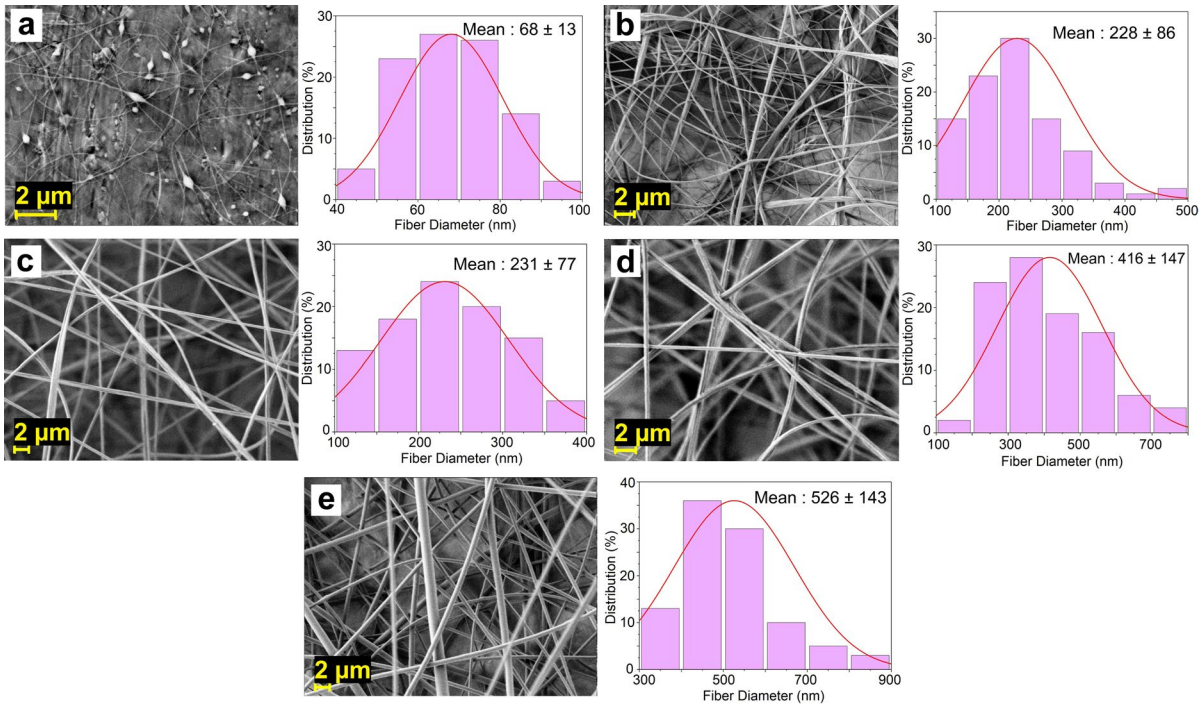

Fig. 7 Scanning electron micrographs and size distribution histograms of EC fibers fabricated by ES: **a** 5EC-EtOH, **b** 10EC-EtOH, **c** 5EC-DMAc:THF, **d** 10EC-DMAc:THF, **e** 15EC-DMAc:THF

engineering or drug delivery involving the release of bioactive or pharmaceutical substances (Kelly et al. 2022).

The equal ratio of DMAc and THF produced fine and bead-free fibers, as shown in Fig. 7c–e, for EC concentrations of 5%, 10%, and 15%, respectively. Unlike ethanol, the combination of DMAc and THF was able to spin EC with a concentration of 15% because the resulting solution's viscosity was low enough for the ES process to be carried out. DMAc and THF thus allowed for the processing of high-concentration polymer solutions. ES at higher polymer concentrations can produce fibers with improved mechanical properties, larger diameter, and enhanced structural integrity (Tarus et al. 2016). This is attributed to a decrease in the number of beads as the solution concentration increases. The presence of beads in the fibers diminishes the number of fiber contact points per unit volume. As the solution concentration increases, smoother fibers with enhanced diameter uniformity are formed, thus increasing the fiber cohesion points and consequently, the tensile strength (Tarus et al. 2020).

It is clear that beads did not appear on the fibers produced from all concentrations tested. DMAc has a slower evaporation rate compared to many other solvents typically used for ES. This slower evaporation rate allows more control over the drying process during ES fabrication. It enables the fibers to solidify more gradually, reducing the risk of rapid drying and bead formation, and facilitating the production of uniform fibers. Moreover, the viscosity and surface tension properties of DMAc and THF contributed to the steady jetting of the EC solution during electrospinning, resulting in well-formed fibers with uniform diameters. The most easily observed difference is the change in the diameter of the resulting fiber. The fibers with a diameter of 231 nm were produced from a 5% EC solution. With the same parameters, the fiber diameter increased to 418 nm when the solution concentration was raised to 10% and increased to 526 nm when the EC solution concentration was 15%. This result indicates that the polymer concentration influences the fiber diameter proportionately, as shown in Fig. 9. Increasing the polymeric solution concentration produces a viscous solution and an

increase in polymer chain entanglements, resulting in a higher fiber diameter (Aulova et al. 2020; Kalluri et al. 2021).

The production rate of ES depends on the solution flow rate applied during the spinning process (Kelly et al. 2022). As a comparison, the 10EC-DMAc:THF was the one with the highest production rate using the PG method, which was 221.4 mg min^{-1}. At a 0.1 mL min^{-1} flow rate, the production rate for spinning 10EC-DMAc:THF by ES was 0.01 mg min^{-1}. This value is much lower than the PG production rate. One of the main weaknesses of typical lab-scale ES is a very low production rate, making it difficult to scale up cellulose fiber production.

Cellulose acetate

All CA solutions were successfully electrospun to produce fibers with different morphologies, as shown in Fig. 8. The combination of acetone and DMAc was able to dissolve all concentrations of CA explored. The surface tension, viscosity, and boiling point of DMAc are all greater than that of acetone. Combining them as a binary solvent system is expected to enhance the properties of the polymer solutions (Wsoo et al. 2020). Figure 8a is a micrograph for the fibers prepared at a concentration of 5%, where it is clear that there are many large beads present. These beads were formed due to insufficient elongational forces that failed to overcome the disruptive forces acting on the jet, resulting in a lack of fiber formation. In this case, the viscosity plays a significant role in Rayleigh instability, when a liquid jet or column breaks up into droplets due to perturbations in its shape (Williams et al. 2018). The interplay of various forces, including surface tension, viscosity, and inertia, influences the stability or instability of the liquid jet. Increasing the concentration to 10% made the resulting fibers bead-free, as shown in Fig. 8b. In accordance with previous results, the resulting average fiber diameter (285 nm) for this concentration was larger than the fibers produced by 5% CA (263 nm). Moreover, at a concentration of 15%, the diameter of the fibers drastically increased to 3.48 µm.

As presented in Fig. 8d, 5CA-DMAc:THF produced fibers with a diameter of 215 nm. However, it can be observed that there are numerous beads in the resulting fibers. By increasing the concentration to 10%, which means there was an increase in the entanglement between the molecular chains, the beads were significantly reduced, although some beading was still observed. With the same ES parameter setup, increasing the CA concentration also produced fibers with a larger diameter of 369 nm. However, at a concentration of 15%, the diameter of the fibers drastically decreased to 144 nm with fine beads. At this concentration, the 20 kV voltage applied to the two previous concentrations was not enough to reach the critical limit, and thus, a higher voltage and lower flow rate had to be used. The electrospinning of 15CA-DMAc:THF could only occur at a voltage of 30 kV with a flow rate of 0.01 mL min^{-1}, which was five times lower.

All different CA concentrations with the solvent system of Ace:DW were also successfully electrospun. Acetone evaporates at a lower temperature than water since its intermolecular forces are fewer and weaker (Wilson et al. 2011). Theoretically, CA is not soluble in water. However, several studies (Crabbe-Mann et al. 2018; Frey 2008) prove that the addition of water to acetone can reduce the evaporation rate of acetone, therefore, it is expected to produce bead-free fibers. The concentration of 5% CA in this solvent system produced thin fibers with an average diameter of 695 nm. Although bead-on strings are still observed in Fig. 8g, the resulting fibers were fine and uniform. This average diameter increased to 962 nm when the CA concentration was increased to 10%. It appears that bead-free fibers were produced at this concentration. Like the other two solvent systems, 15CA-Ace:DW required higher voltage and lower flow rate for the ES process. Although the morphology was similar to 15CA-Ace:DMAc and 15CA-DMAc:THF, the resulting fiber diameter was slightly larger at 187 nm. Although the fibers' quality tended to be better than the two previous solvent systems, the diameter of the fibers produced by this solvent system was relatively larger.

Overall, apart from the 15% concentration, which required different parameters, increasing the solution concentration affected the diameter of the fibers produced. As with EC, the larger the solution, the more fibers with a larger diameter were produced, as shown in Fig. 9. These results are like those obtained by the PG method. An increased polymer concentration, resulting in a reduced proportion of solvents, accelerates solvent evaporation. This, in turn, restricts the stretching effect caused by electrostatic and columbic

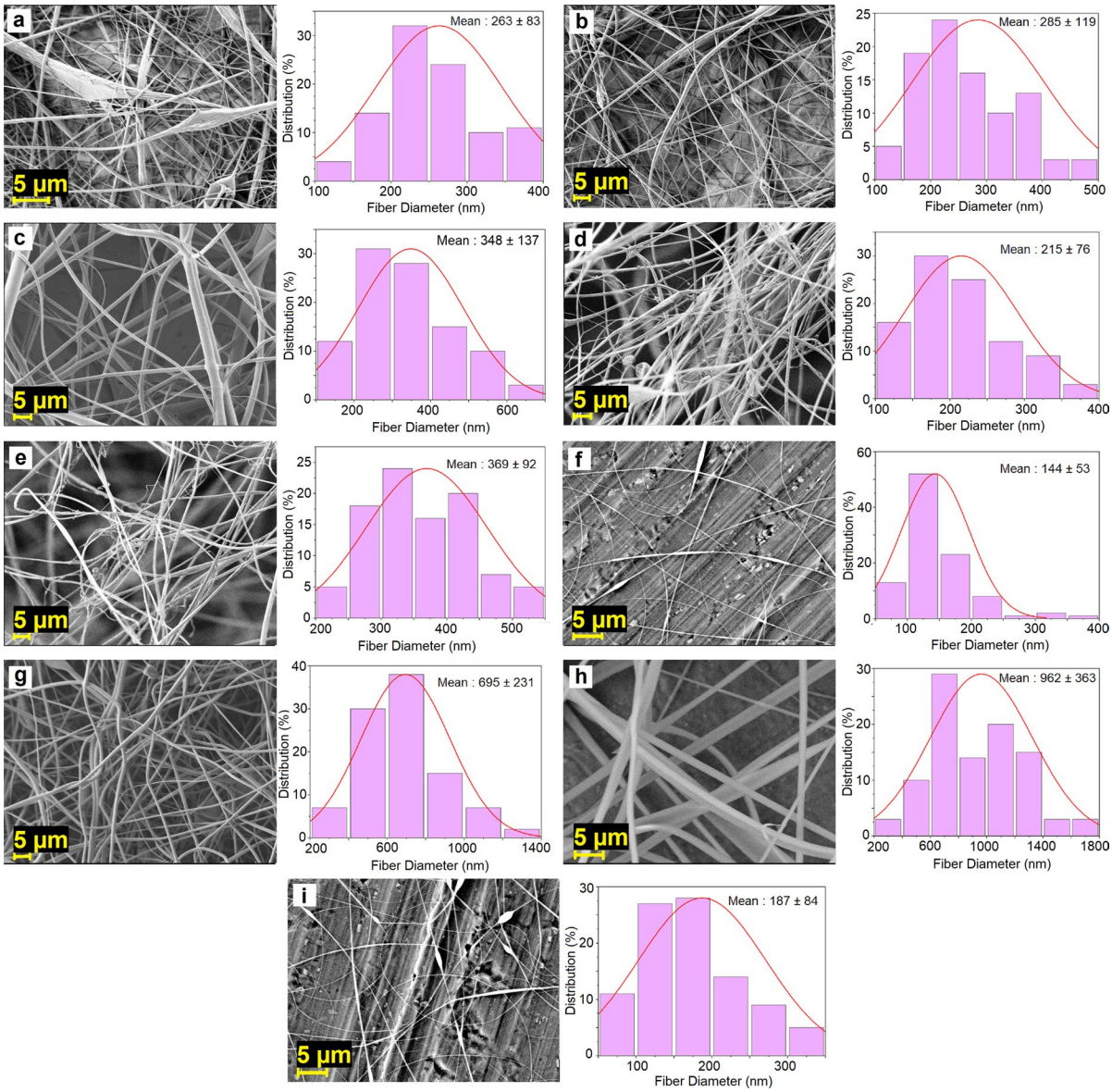

Fig. 8 Scanning electron micrographs and size distribution histograms of the CA fibers fabricated by ES: **a** 5CA-Ace:DMAc, **b** 10CA-Ace:DMAc, **c** 15CA-Ace:DMAc, **d** 5CA-DMAc:THF, **e** 10CA-DMAc:THF, **f** 15CA-DMAc:THF, **g** 5CA-Ace:DW, **h** 10CA-Ace:DW, **i** 15CA-Ace:DW

repulsion forces, leading to the formation of fibers with a larger diameter (Sriyanti et al. 2020; Tarus et al. 2020).

Fourier transform infrared spectroscopy (FTIR)

FTIR spectroscopy was performed to explore differences in the chemical nature of the EC fibers produced by PG and ES. A comparison of the characteristics of the absorption bands of EC powder and EC fiber is shown in Fig. 10. In the powder form, the EC spectrum had distinct bands at 1054 and 1375 cm^{-1}, which correspond to the stretching of C–O–C bonds and the bending of –CH groups, respectively (Godakanda et al. 2019). The bands observed at 2973 and 2872 cm^{-1} were the results of

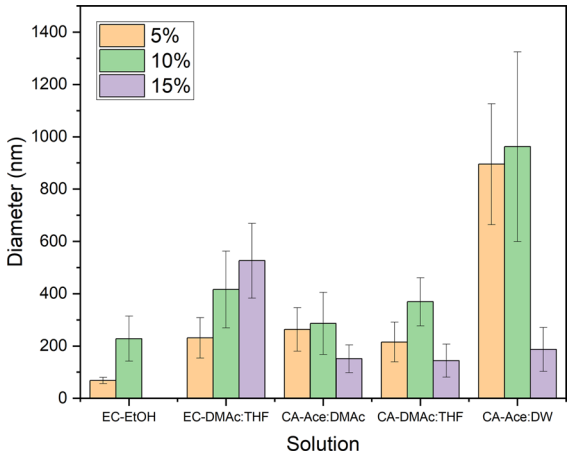

Fig. 9 The effect of solution concentration on the diameter of fibers

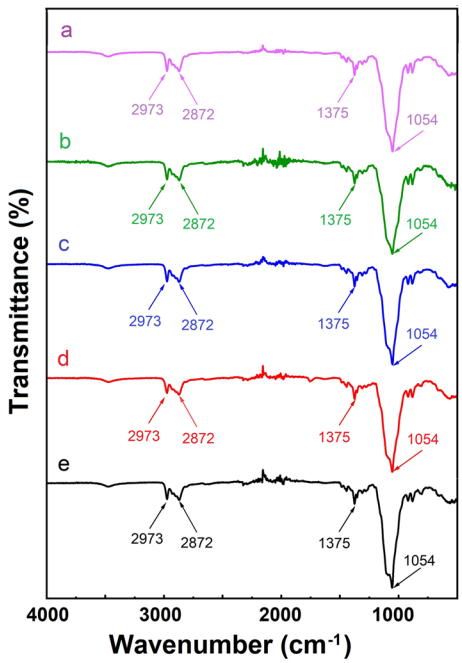

Fig. 10 FTIR spectra of: **a**. EC powder, **b**. 10EC-DMAc:THF pressure-spun fiber, **c**. 15EC-DMAc:THF pressure-spun fiber, **d**. 10EC-DMAc:THF electrospun fiber, and **e**. 15EC-DMAc:THF electropun fiber

the stretching vibrations of the C–C present in alkyl groups of EC (Paulo et al. 2022). The identical spectra were also shown by pressure-spun and electrospun fibers for both concentrations (10EC-DMAc:THF and 15EC-DMAc:THF). These characteristics indicated that the different spinning methods did not affect IR absorption and chemical structures. Those spectra also agree with the EC spectrum reported in the literature (Biswas et al. 2013; Gunduz et al. 2013).

X-Ray diffraction (XRD)

XRD tests were conducted to observe the physical form of the raw material (EC powder) and the fibers generated by PG and ES. Figure 11a illustrates that the pattern of EC exhibits a broad halo, suggesting that it is predominantly composed of amorphous material. However, a distinct and well-defined reflection at approximately 11.15° indicates that the polymer has a somewhat crystalline structure. This result is in agreement with the literature (Geng and Williams 2023). After spinning, irrespective of the techniques employed, all the fibers (10EC-DMAc:THF and 15EC-DMAc:THF) exhibit

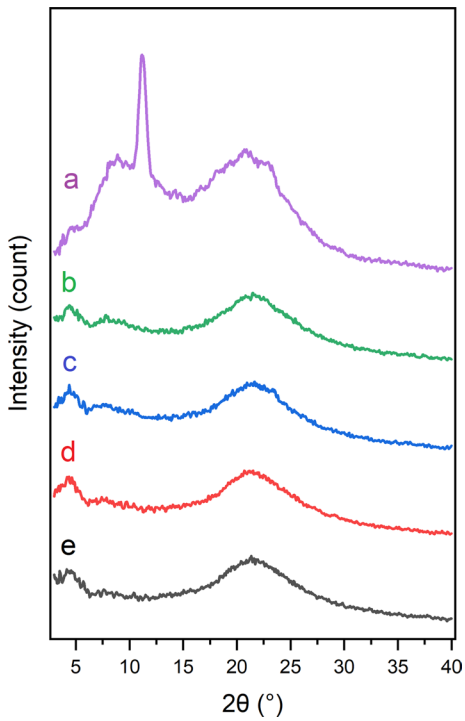

Fig. 11 XRD data of: **a**. EC powder, **b**. 10EC-DMAc:THF pressure-spun fiber, **c**. 15EC-DMAc:THF pressure-spun fiber, **d**. 10EC-DMAc:THF electrospun fiber, and **e**. 15EC-DMAc:THF electropun fiber

only wide haloes in their patterns (Fig. 11b–e). The broad peaks of the electrospun and pressure-spun fiber diffractograms are observed to be around 4.7°, 8.1°, and 21.3°, indicating that both the electrospun and pressure-spun fibers possessed an amorphous structure. The explanation for this finding lies in the amorphization occurring during the spinning process. As the precursor solution is drawn towards the collector and elongated, it undergoes a transition from liquid to solid state. Throughout this transformation, solvent molecules evaporate, leaving the polymer molecules bonded more tightly together, with their bonds strengthening. This phenomenon is driven by ionic motion, which is expedited by an electric field, occurring rapidly enough that EC molecules are unable to align themselves to form a crystalline structure (Sriyanti et al. 2020).

Differential scanning calorimetry (DSC)

Differential scanning calorimetry (DSC) investigations were undertaken to observe and compare the thermal properties of EC pressure-spun and electrospun fibers. Figure 12 depicts the thermographs of EC powder and fibers fabricated. As confirmed in the XRD result, EC is considered to be an entirely amorphous material. In the literature (Lai et al. 2010), its glass transition temperature (Tg) is in the range of 130–150 °C. However, the specific value of Tg seems to vary depending on the kind of EC and the method of measurement employed. Moreover, the exothermic peak observed at 174 °C is most likely attributed to the crystallization of EC (Geng and Williams 2023).

Figure 12b and c present the DSC traces of 10EC-DMAc:THF and 15EC-DMAc:THF pressure-spun fibers, respectively. It is seen that the exothermic peak shifts to 183 °C for both concentrations. With the different method, electrospinning, an increase in the exothermic peak is also observed at 177 °C for both 10EC-DMAc:THF (Fig. 12d) and 15EC-DMAc:THF (Fig. 12e). The shifting of the peak in the fiber form of EC to higher temperatures can be attributed to a promoted rapid crystallization during spinning process. This is the intrinsic nature of the rapid formation of structures in the PG and ES process that inherently leads to inadequate time

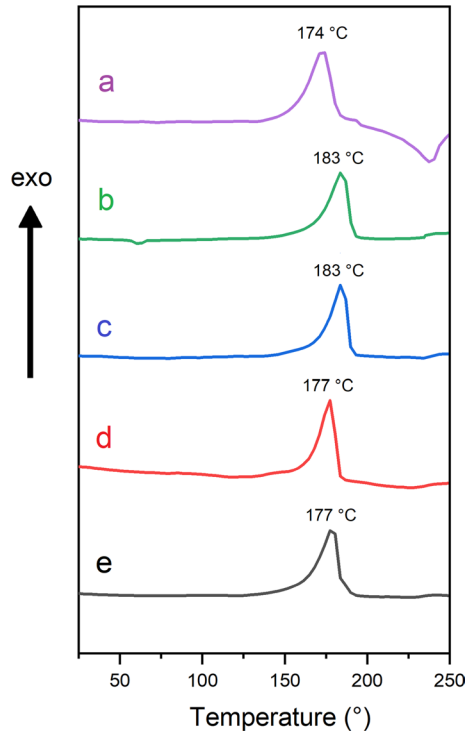

Fig. 12 DSC thermograms of: **a**. EC powder, **b**. 10EC-DMAc:THF pressure-spun fiber, **c**. 15EC-DMAc:THF pressure-spun fiber, **d**. 10EC-DMAc:THF electrospun fiber, and **e**. 15EC-DMAc:THF electropun fiber

for the formation of perfect crystallites in the EC matrix compared to the bulk (Kim 2010).

Conclusions

The research demonstrates a novel industrial approach to successfully mass-produce cellulose derivative fibers for the first time. The behaviors of EC and CA varied across the three spinning methods investigated in this study: PG, N-PG, and ES. The results showed that EC, when utilizing a binary solvent system of DMAc:THF, was the only successfully spun cellulose derivative using PG and N-PG. The N-PG produced more aligned fibers, indicated by the higher coherency coefficient than PG. The optimization of PG by applying different gas pressures and gyration speeds revealed that the higher the gas pressure or the gyration speed, the smaller the diameter of the resulting fibers. Both EC and CA were successfully electrospun, and bead-free fibers can be produced by increasing

the concentration of the solution to improve polymer chain entanglement. However, under the same spinning parameters, an increase in the solution concentration tended to increase the diameter of the resulting fibers. A comparison of pressure-spun and electrospun fibers through FTIR, XRD, and DSC analyses showed that neither method caused any significant changes in the physicochemical nature of the polymer, and both were amorphous. Despite the challenges associated with the PG method, the successful production of fibers using this method shows its potential for future applications. Further investigations, such as process optimization, understanding the rheological behavior of cellulose derivatives under pressure, appropriate solvent selection, and a comprehensive characterization of the resulting fibers, could position this method as a promising alternative for producing cellulose fibers with a high production rate.

Acknowledgments The authors wish to give thanks to Margarita Strimaite (UCL School of Pharmacy) for her assistance with XRD. Yanqi Dai (Department of Mechanical Engineering, UCL) is also credited with providing a N-PG spinning vessel.

Author contributions NQ conceptualization, investigation, formal analysis, writing—original draft. HM investigation, formal analysis, writing—reviewing. JA writing—reviewing. GW conceptualization, supervision, writing—reviewing. ME conceptualization, supervision, writing—reviewing.

Funding NQ would like to thank LPDP, The Ministry of Finance, The Republic of Indonesia, for funding his PhD study at UCL.

Data availability The data that support the findings of this study are available from the corresponding author upon reasonable request.

Declarations

Competing interest There are no relevant financial or non-financial interests of the authors to disclose.

Ethical approval Not applicable.

Consent for publication All authors agree to publish this work.

References

Ajith G, Tamilarasi GP, Sabarees G, Gouthaman S, Manikandan K, Velmurugan V, Alagarsamy V, Solomon VR (2023) Recent developments in electrospun nanofibers as delivery of phytoconstituents for wound healing. Drug Drug Cand 2(1):148–171. https://doi.org/10.3390/ddc2010010

Altun E, Aydogdu MO, Koc F, Crabbe-Mann M, Brako F, Kaur-Matharu R, Ozen G, Kuruca SE, Edirisinghe U, Gunduz O (2018) Novel making of bacterial cellulose blended polymeric fiber bandages. Macromol Mater Eng 303(3):1700607. https://doi.org/10.1002/mame.201700607

Angel N, Guo L, Yan F, Wang H, Kong L (2020) Effect of processing parameters on the electrospinning of cellulose acetate studied by response surface methodology. J Agri Food Res 2:100015. https://doi.org/10.1016/j.jafr.2019.100015

Aulova A, Bek M, Kossovich L, Emri I (2020) Needleless electrospinning of PA6 fibers: the effect of solution concentration and electrospinning voltage on fiber diameter. Stroj Vestn j Mech Eng 66(7–8):421–430. https://doi.org/10.5545/sv-jme.2020.6713

Biswas A, Kim S, Selling G, Cheng H (2013) Microwave-assisted synthesis of alkyl cellulose in aqueous medium. Carbohyd Polym 94(1):120–123. https://doi.org/10.1016/j.carbpol.2013.01.022

Brako F, Raimi-Abraham BT, Mahalingam S, Craig DQ, Edirisinghe M (2018) The development of progesterone-loaded nanofibers using pressurized gyration: a novel approach to vaginal delivery for the prevention of preterm birth. Int J Pharm 540(1–2):31–39. https://doi.org/10.1016/j.ijpharm.2018.01.043

Chavooshi R, Ranjkesh MR, Hashemi B, Roshangar L (2023) Cellulose and lignin-derived scaffold and their biological application in tissue engineering, drug delivery, and wound healing: a review. Cell J 25(3):158. https://doi.org/10.22074/CELLJ.2023.559011.1095

Chen Y, Qiu Y, Chen W, Wei Q (2020) Electrospun thymol-loaded porous cellulose acetate fibers with potential biomedical applications. Mater Sci Eng C 109:110536. https://doi.org/10.1016/j.msec.2019.110536

Crabbe-Mann M, Tsaoulidis D, Parhizkar M, Edirisinghe M (2018) Ethyl cellulose, cellulose acetate and carboxymethyl cellulose microstructures prepared using electrohydrodynamics and green solvents. Cellulose 25:1687–1703. https://doi.org/10.1007/s10570-018-1673-y

Dadol GC, Lim KJA, Cabatingan LK, Tan NPB (2020) Solution blow spinning–polyacrylonitrile–assisted cellulose acetate nanofiber membrane. Nanotechnology 31(34):345602. https://doi.org/10.1088/1361-6528/ab90b4

Dai Y, Ahmed J, Delbusso A, Edirisinghe M (2022) Nozzle-pressurized gyration: a novel fiber manufacturing process. Macromol Mater Eng 307(9):2200268. https://doi.org/10.1002/mame.202200268

Dai Y, Ahmed J, Edirisinghe M (2023) Pressurized gyration: fundamentals, advancements, and future. Macromol Mater Eng 308(7):2300033. https://doi.org/10.1002/mame.202300033

Dai Y, Sun D, Sundaram S, Delbusso A, O'Rourke D, Dorris M, Edirisinghe M (2024) Facile synthesis: from laminaria hyperborea to cellulose films and fibers. Cellulose 31(1):205–216. https://doi.org/10.1007/s10570-023-05606-w

Frey MW (2008) Electrospinning cellulose and cellulose derivatives. Polym Rev 48(2):378–391. https://doi.org/10.1080/15583720802022281

Gençtürk A, Kahraman E, Güngör S, Özsoy Y, Sarac AS (2020) Effects of polyvinylpyrrolidone and ethyl cellulose in polyurethane electrospun nanofibers on morphology and drug release characteristics. Turk J Pharm Sci 17(6):638. https://doi.org/10.4274/tjps.galenos.2019.87094

Geng Y, Williams GR (2023) Developing and scaling up captopril-loaded electrospun ethyl cellulose fibers for sustained-release floating drug delivery. Int J Pharm 648:123557. https://doi.org/10.1016/j.ijpharm.2023.123557

Godakanda VU, Li H, Alquezar L, Zhao L, Zhu LM, de Silva R, de Silva KN, Williams GR (2019) Tunable drug release from blend poly (vinyl pyrrolidone)-ethyl cellulose nanofibers. Int J Pharm 562:172–179. https://doi.org/10.1016/j.ijpharm.2019.03.035

Gunduz O, Ahmad Z, Stride E, Edirisinghe M (2013) Continuous generation of ethyl cellulose drug delivery nanocarriers from microbubbles. Pharm Res 30:225–237. https://doi.org/10.1007/s11095-012-0865-7

Heseltine PL, Ahmed J, Edirisinghe M (2018) Developments in pressurized gyration for the mass production of polymeric fibers. Macromol Mater Eng 303(9):1800218. https://doi.org/10.1002/mame.201800218

Husain O, Lau W, Edirisinghe M, Parhizkar M (2016) Investigating the particle to fibre transition threshold during electrohydrodynamic atomization of a polymer solution. Mater Sci Eng C 65:240–250. https://doi.org/10.1016/j.msec.2016.03.076

Jayawardena B, Pandithavidana DR, Sameera W (2017) Polysaccharides in solution: experimental and computational studies solubility of polysaccharides. IntechOpen. https://doi.org/10.5772/intechopen.69863

Kalluri L, Satpathy M, Duan Y (2021) Effect of electrospinning parameters on the fiber diameter and morphology of PLGA nanofibers. Dent Oral Biol Cranio Res. https://doi.org/10.31487/j.dobcr.2021.02.04

Kelly A, Ahmed J, Edirisinghe M (2022) Manufacturing cyclodextrin fibers using water. Macromol Mater Eng 307(6):2100891. https://doi.org/10.1002/mame.202100891

Kim G-M (2010) Fabrication of bio-nanocomposite nanofibers mimicking the mineralized hard tissues via electrospinning process. Nanofibers. https://doi.org/10.5772/8148

Lai HL, Pitt K, Craig DQ (2010) Characterisation of the thermal properties of ethylcellulose using differential scanning and quasi-isothermal calorimetric approaches. Int J Pharm 386(1–2):178–184. https://doi.org/10.1016/j.ijpharm.2009.11.013

Mahalingam S, Edirisinghe M (2013) Forming of polymer nanofibers by a pressurised gyration process. Macromol Rapid Comm 34(14):1134–1139. https://doi.org/10.1002/marc.201300339

Mahalingam S, Huo S, Homer-Vanniasinkam S, Edirisinghe M (2020) Generation of core–sheath polymer nanofibers by pressurised gyration. Polymers 12(8):1709. https://doi.org/10.3390/polym12081709

Mahalingam S, Raimi-Abraham BT, Craig DQ, Edirisinghe M (2015) Solubility–spinnability map and model for the preparation of fibres of polyethylene (terephthalate) using gyration and pressure. Chem Eng J 280:344–353. https://doi.org/10.1016/J.CEJ.2015.05.114

Mehta PP, Pawar VS (2018) Electrospun nanofiber scaffolds: technology and applications applications of nanocomposite materials in drug delivery. Elsevier. https://doi.org/10.1016/B978-0-12-813741-3.00023-6

Oprea M, Voicu SI (2020) Recent advances in composites based on cellulose derivatives for biomedical applications. Carbohyd Polym 247:116683. https://doi.org/10.1016/j.carbpol.2020.116683

Paulo F, Tavares L, Santos L (2022) Extraction and encapsulation of bioactive compounds from olive mill pomace: influence of loading content on the physicochemical and structural properties of microparticles. J Food Meas Charact 16(4):3077–3094. https://doi.org/10.1007/s11694-022-01408-z

Rao J, Shen C, Yang Z, Fawole OA, Li J, Wu D, Chen K (2022) Facile microfluidic fabrication and characterization of ethyl cellulose/PVP films with neatly arranged fibers. Carbohyd Polym 292:119702. https://doi.org/10.1016/j.carbpol.2022.119702

Rezakhaniha R, Agianniotis A, Schrauwen JTC, Griffa A, Sage D, Bouten VC, Vosse FVD, Unser M, Stergiopulos N (2012) Experimental investigation of collagen waviness and orientation in the arterial adventitia using confocal laser scanning microscopy. Biomech Model Mechanobiol 11:461–473. https://doi.org/10.1007/s10237-011-0325-z

Seddiqi H, Oliaei E, Honarkar H, Jin J, Geonzon LC, Bacabac RG, Klein-Nulend J (2021) Cellulose and its derivatives: towards biomedical applications. Cellulose 28(4):1893–1931. https://doi.org/10.1007/s10570-020-03674-w

Shaghaleh H, Xu X, Wang S (2018) Current progress in production of biopolymeric materials based on cellulose, cellulose nanofibers, and cellulose derivatives. RSC Adv 8(2):825–842. https://doi.org/10.1039/c7ra11157f

Sofi HS, Akram T, Shabir N, Vasita R, Jadhav AH, Sheikh FA (2021) Regenerated cellulose nanofibers from cellulose acetate: Incorporating hydroxyapatite (HAp) and silver (Ag) nanoparticles (NPs), as a scaffold for tissue engineering applications. Mater Sci Eng C 118:111547. https://doi.org/10.1016/j.msec.2020.111547

Sriyanti I, Agustini MP, Jauhari J, Sukemi S, Nawawi Z (2020) Electrospun nylon-6 nanofibers and their characteristics. J Ilm Pendidik Fis Al-Biruni 9(1):9–19. https://doi.org/10.24042/jipfalbiruni.v9i1.5747

Tarus B, Fadel N, Al-Oufy A, El-Messiry M (2016) Effect of polymer concentration on the morphology and mechanical characteristics of electrospun cellulose acetate and

poly (vinyl chloride) nanofiber mats. Alexandria Eng J 55(3):2975–2984. https://doi.org/10.1016/j.aej.2016.04.025

Tarus BK, Fadel N, Al-Oufy A, El-Messiry M (2020) Investigation of mechanical properties of electrospun poly (vinyl chloride) polymer nanoengineered composite. J Eng Fiber Fabr 15:1558925020982569. https://doi.org/10.1177/1558925020982569

Wang H, Liao S, Bai X, Liu Z, Fang M, Liu T, Wang N, Wu H (2016) Highly flexible indium tin oxide nanofiber transparent electrodes by blow spinning. ACS Appl Mater Inter 8(48):32661–32666. https://doi.org/10.1021/acsami.6b13255

Wang Y, Gao M, Pan X, He Y, Liu Y, Ji M, Si T, Sun Y (2023) Preparation of resveratrol-loaded ethyl cellulose microspheres via foam-transfer and its application performances. Cellulose 30:6401–6421. https://doi.org/10.1007/s10570-023-05274-w

Williams GR, Raimi-Abraham BT, Luo C (2018) Nanofibres in drug delivery. UCL Press, London

Wilson C, Borgmeyer B, Winholtz R, Ma H, Jacobson D, Hussey D (2011) Thermal and visual observation of water and acetone oscillating heat pipes. J Heat Transf. https://doi.org/10.1115/1.4003546

Wsoo MA, Shahir S, Bohari SPM, Nayan NHM, Abd Razak SI (2020) A review on the properties of electrospun cellulose acetate and its application in drug delivery systems: a new perspective. Carbohyd Res 491:107978. https://doi.org/10.1016/j.carres.2020.107978

Wu X, Zhang L, Zhang X, Zhu Y, Wu Y, Li Y, Li B, Liu S, Zhao J, Ma Z (2017) Ethyl cellulose nanodispersions as stabilizers for oil in water Pickering emulsions. Sci Rep 7(1):12079. https://doi.org/10.1038/s41598-017-12386-4

Young RE, Graf J, Miserocchi I, Van Horn RM, Gordon MB, Anderson CR, Sefcik LS (2019) Optimizing the alignment of thermoresponsive poly (N-isopropyl acrylamide) electrospun nanofibers for tissue engineering applications: a factorial design of experiments approach. PLoS ONE 14(7):e0219254. https://doi.org/10.1371/journal.pone.0219254